Available online at www.sciencedirect.com
ScienceDirect
Microporous and Mesoporous Materials 95 (2006) 164–171
MICROPOROUS AND MESOPOROUS MATERIALS
www.elsevier.com/locate/micromeso

Evaluation of self-organized diffusion barrier continuity on a nano-architectural silica thin film with two-dimensionally connected cage-like pores using positronium time of flight spectroscopy

H.K.M. Tanaka [a,b,*], T. Kurihara [c], N. Nishiyama [d], T. Maruo [d], A.P. Mills Jr. [a]

[a] *Physics Department, University of California, Riverside, Riverside, CA 92521, USA*
[b] *Muon Science Laboratory, Institute of Materials Structure Science (IMSS), High Energy Accelerator Research Organization (KEK), 1-1 Oho, Tsukuba, Ibaraki 305-0801, Japan*
[c] *Slow Positron Facility, Institute of Materials Structure Science (IMSS), High Energy Accelerator Research Organization (KEK), 1-1 Oho, Tsukuba, Ibaraki 305-0801, Japan*
[d] *Division of Chemical Engineering, Graduate School of Engineering Science, Osaka University, 1-3 Machikaneyama, Toyonaka, Osaka 560-8531, Japan*

Received 26 August 2005; received in revised form 27 April 2006; accepted 4 May 2006
Available online 7 July 2006

Abstract

Positronium time of flight (Ps-TOF) was measured by implanting slow positron pulses at variable energies into a nano-architectural silica thin film with two-dimensionally connected cage-like pores to investigate a continuity of the self-organized extremely thin diffusion barrier between the pores. By comparing a capped and open-pored low-k film, we found a Ps-TOF spectrum with positron implantation energy of 0.2 keV that reflects the sample structure is consistent with an open pore fraction $\eta < 1.7 \cdot \times 10^{-6}$ of the diffusion barrier.

Keywords: Positronium; Time of flight spectroscopy; Self-organization; Mesoporous silica; Low-k interlayer dielectrics

1. Introduction

Submicron thin films of porous silica and organosilicates are vigorously being developed as low-dielectric (low-k), interlayer insulators for use in high-speed microelectronic devices [1]. The integration of copper with porous ultralow-k interlayer dielectrics (ILDs) is required to overcome the resistance–capacitance (RC) time delay of integrated circuits and crosstalk noise problems for future generation computer microprocessors [2–6]. However, Cu is known to have high diffusivity into most of the promising ILD materials, and the presence of Cu in the pores of low-k materials results in serious device degradation and failure. Therefore, it is necessary to separate the Cu interconnect lines from the surrounding ILD by diffusion barriers [7] Positronium annihilation lifetime spectroscopy (PALS) has been applied to determine whether or not a diffusion barrier on an open-pored low-k film is impervious [8–11]. A Ta barrier only 5 nm thick is not completely effective in preventing Ps diffusion out of a low-k film [12]. On the other hand, a capping layer of 80 nm silica effectively blocks the diffusion of Ps out of a low-k film [9]. Although PALS measurement has been useful to measure the diffusion of the positronium out of a supported thin film, it has limitations in measuring a diffusivity or an open pore fraction of the diffusion barrier. Ps-TOF spectroscopy may be a unique technique to offer direct information about the atoms that diffuse out of a low-k thin film.

In the last several years, positronium time of flight spectroscopy (Ps-TOF) has become an established technique for probing Ps emission from surface or Ps diffusion in

* Corresponding author. Address: Physics Department, University of California, Riverside, Riverside, CA 92521, USA. Tel.: +1 951 827 5331; fax: +1 951 827 4529.
E-mail address: hiroyuki@physics.ucr.edu (H.K.M. Tanaka).

1387-1811/$ - see front matter
doi:10.1016/j.micromeso.2006.05.011

matter [13,14]. If the small pinholes or discontinuities in the barrier itself form a passage allowing Ps to escape into vacuum, this effect can be easily detected by Ps-TOF spectroscopy. Ps-TOF spectroscopy might be a complementary method to obtain further understanding by separating decays in the porous matrix from decays attributed to Ps escape into vacuum. Recently we found that a spin-coated capping layer of 50 nm silica confine Ps atoms. However, it is difficult to make a diffusion barrier thinner than 50 nm by spin coating method. Much thinner and effective barrier is strongly required.

Preparation of thin films of mesoporous materials [15–22] has attracted considerable attention because of their possible applications in the fields of separations, chemical sensors, optical devices, and electronic devices such as low-k dielectric films. The mesoporous materials contain several unique structures: lamellar (MCM-50 [23]), cubic *Pm3n* (SBA-1 [24]), cubic *Ia3d* (MCM-48 [23]), two-dimensional hexagonal *P6m* (FSM-16, [25] MCM-41, [23] SBA-3, [24] and SBA-15 [26]), and three-dimensional hexagonal $P6_3/mmc$ (SBA-2 [24]). The desired mesostructures of the silica materials have conventionally been obtained by controlling the composition and pH of a precursor solution and synthetic time and temperature. The geometric structures are based on the idea of a surfactant packing parameter [27]. Moreover, several phase transitions from one kind of mesostructure to another are found under drying [27,28] and hydrothermal conditions [29].

In contrast, we have first found phase transition of surfactantsilicate nano-composites under vapor-phase synthesis [30]. Cetyltrimethylammonium bromide (C_{16}TAB) films on a Si substrate were treated with tetraethoxysilane (TEOS) and tetramethoxysilane (TMOS). The obtained films have hexagonally arranged pore channels that run parallel to the film surface. However, when the films are used as electric devices, the structure of pores of the films should be isotropic parallel to the surface in some cases. In vapor-phase method, selection of surfactant is the most important factor to determine the porous structure similarly to the sol–gel method [31]. In this work, we used the Ps-TOF spectrometer developed at Slow Positron Facility, High Energy Accelerator Organization (KEK-SPF) to investigate the self-organized diffusion barrier produced in a nano-architectural silica thin film with two-dimensionally connected cage-like pores by comparing the Ps-TOF spectrum in a capped and open-pored low-k film.

2. Experimental

Our apparatus consists of a pulsed source of slow positrons, a capped and open pored spin-on low-k film and a new mesostructured film at room temperature, a time of flight spectrometer for measuring Ps velocities, and associated electronics. The present experiment was performed at Slow Positron Facility, High Energy Accelerator Research Organization [32]. The facility consists of a 50 MeV linac, an assembly of slow positron generator, a slow positron transport line and an experimental station for positron time of flight (Ps-TOF) spectroscopy. Fig. 1 shows an overview of the facility. The experimental setup is shown

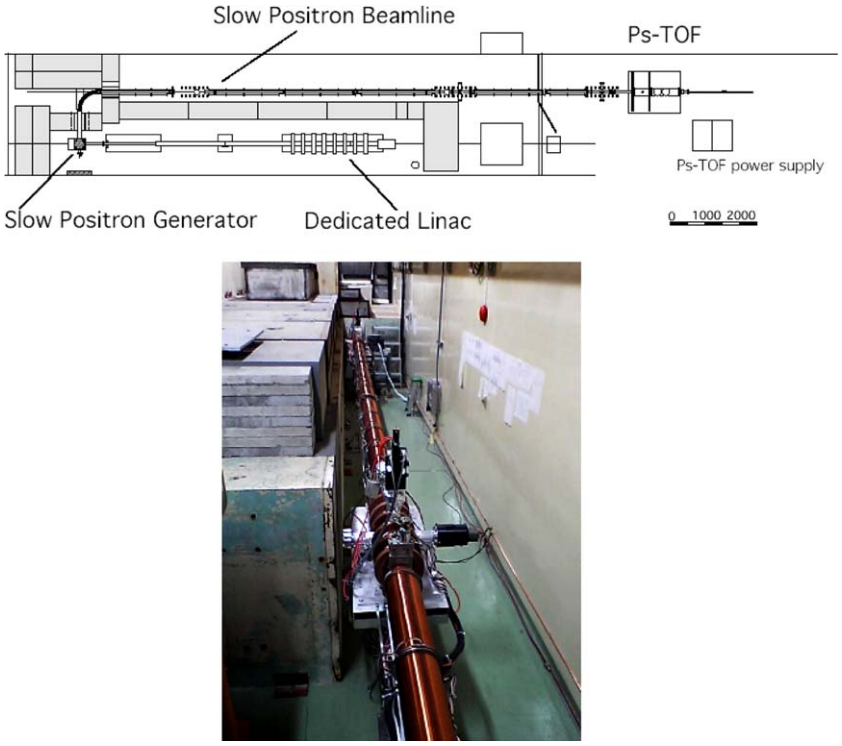

Fig. 1. Schematic view of 50 MeV linac, an assembly of slow positron generator, a slow positron transport line and an experimental station for positron time of flight (Ps-TOF) spectroscopy: (upper) drawing; (lower) photograph.

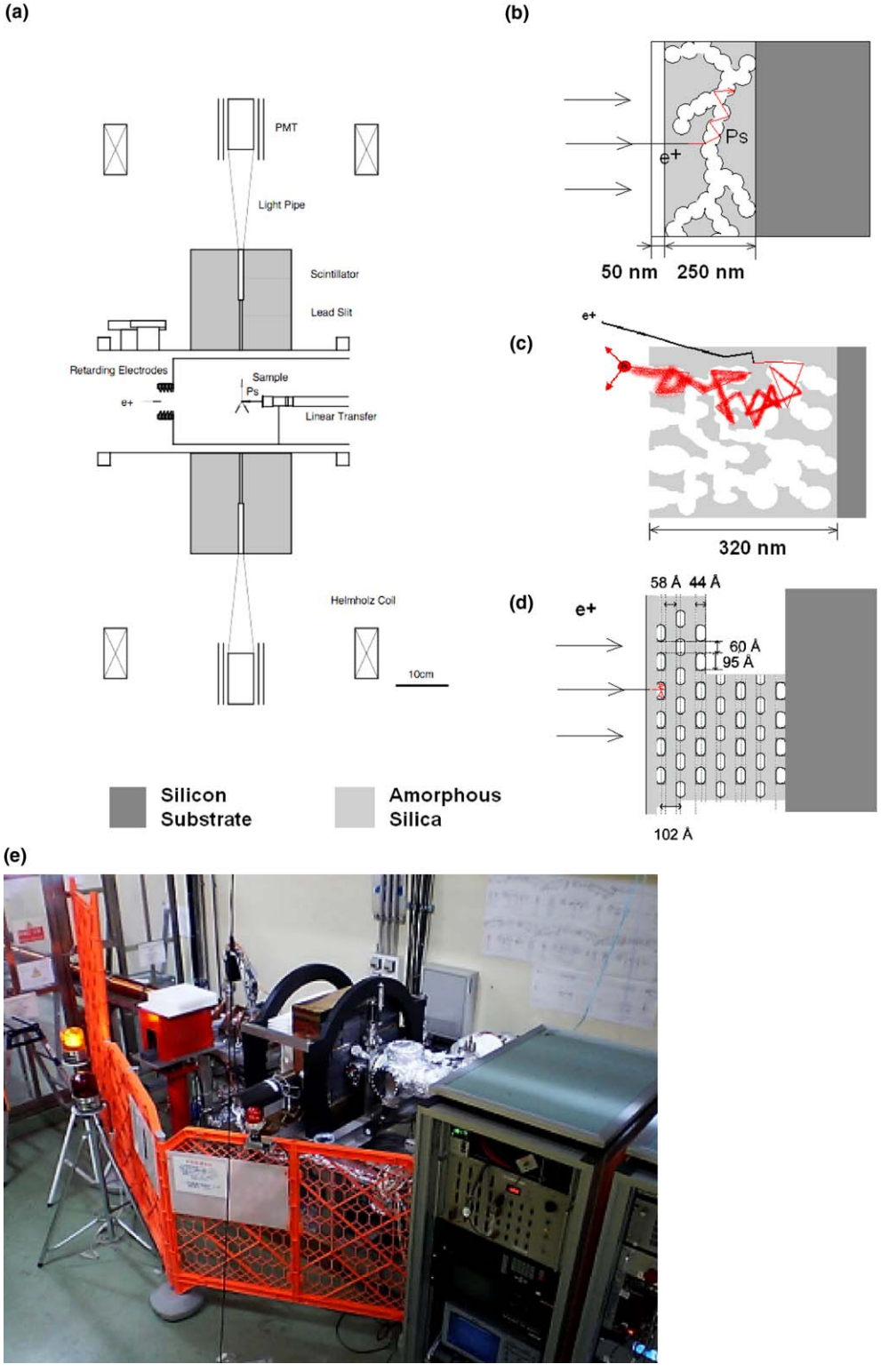

Fig. 2. (a) Principle of Ps-TOF measurement experiment; conceptual view of the preset samples: (b) a capped, (c) an open-pored, and (d) a mesostructured low-k film; (e) Ps-TOF measurement experimental setup.

in Fig. 2. The principle of the Ps-TOF method has been previously discussed [33], and is only briefly introduced here. In the TOF measurement, the sample is bombarded with a slow positron beam. The time interval between the linac signal and the detection of the gamma ray from the emitted o-Ps self-annihilation is measured to obtain the energy distribution of the emitted Ps. In the present experiment, the lead collimator was adjusted to

effectively reduce the annihilation gamma rays from the sample region to detect only the decay events from self-annihilation of Ps in the view of the plastic scintillator through a 4.5 mm lead slit. And at the same time, however, the counter also detects a part of the decay events after passing through the lead shield from the sample region (the decay events from the sample are not totally shielded by the lead blocks). If the diffusion barrier is not impervious, Ps can diffuse out of the film and it can be easily detected by the Ps-TOF spectrometer.

We performed a Ps-TOF measurement experiment at the downstream end of the beam line. The pulse heights and annihilation gamma rays and the time when annihilation events occur are recorded by a digital oscilloscope (LeCroy Wavepro 960). A pulse fed from the linac triggered the start. The scintillator was 600 mm in diameter and 10 mm in thickness and was coupled on opposite sides to a photomultiplier tube (HAMAMATSU H 1949) through a Lucite light guide. The vacuum level in the sample chamber was kept to be 10^{-8}–10^{-9} torr throughout the present experiment period. The sample bias can be varied in the range of 0–9 keV by changing the electric potential at the sample by using a retarding element (RET). The energy of the slow positron beam is 5 keV. The beam size was 1 cm in diameter. The beam intensity and the pulse width were 2×10^5 positrons/pulse and 22 ns, respectively.

Mesostructured silica films were prepared according to the reported method [31]: A silicon wafer was cut into 2×2 cm^2 pieces and used as a substrate. Nonionic poly (ethylene oxide)–poly(propylene oxide)–poly(ethylene oxide) amphiphilic triblock copolymer ($EO_{106}PO_{70}EO_{106}$; Pluronic F127) was used as a templating agent. The surfactant film was prepared on the silicon wafer by spin-coating using a solution of Pluronic F127, ethanol (EtOH), HCl and deionized water (the mole ratios: 0.03 Pluronic F127:100EtOH:100H_2O:0.1HCl). The surfactant film was placed vertically in a closed vessel (200 cm^3) along with a separate, small amount of TEOS and HCl (5 N). The vessel was then placed in an oven at 90 °C for 60 min. Thus, the surfactant film was exposed to a saturated TEOS vapor under autogenous pressure. The film was calcined at 400 °C in air for 5 h with a heating rate of 1 °C/min. The products were identified by XRD patterns recorded on a Philips X' Pert-MPD using Cu-Kα radiation with $\lambda = 1.5418$ Å in the θ–2θ scan mode. FE-SEM images were recorded on a Hitachi S-5000L microscope at an acceleration voltage of 21 kV. No coating was carried out for the samples before the FE-SEM measurements. TEM images of a calcined mesoporous silica film were recorded on a Hitachi H9000 electron microscope at an acceleration voltage of 300 kV. The N_2 adsorption/desorption isotherms of products were measured at 77 K using an AUTOSORB-1 instrument (Quantachrome Co.). The measurements were performed with powdery sample, which was peeled from the Si substrate. The pore size distributions were calculated using the BJH model from the desorption branch. The pore volume was determined from the adsorption branch of the N_2 isotherm curve at $P/P_0 = 0.983$. The surface area was calculated by the BET method.

The FE-SEM images of the cross-section of the mesoporous silica film revealed a plausible structure of the mesoporous silica film on the silicon substrate. Hexagonally arranged stubbed pillars were found on the substrate surface. The mesoporous silica film consists of layered silica parallel to the film surface with periodic pillars. The mesostructures of the thin film are summarized in Fig. 2(d): the lattice spacing d of 102 Å, silica layer thickness of 58 Å, and pillar diameter in the middle of 60 Å. The film has twenty layers and was about 200-nm thick. The pores at the film–substrate interface are hemisphere in shape. Nano-pores look like ellipsoidal structures whose diameter along the lateral axis (95 Å) is longer than the one along the longitudinal axis (44 Å). The properties of the present mesostrutured sample are summarized in Table 1.

The XRD pattern of the mesoporous silica film calcined at 400 °C showed a large 1 0 0 reflection corresponding to the lattice spacing $d =$ 102.0 Å. The BET surface area of the mesoporous silica film, calculated by assuming the covered area by nitrogen molecules as 0.162 nm^2, was 720 m^2/g. The mesoporous silica film shows a sharp pore size distribution, with a pore diameter of 72 Å. The o-Ps lifetime of 60 ns, as obtained by assuming the rigid spherical potential model [34] is long enough to see the effect in a pore with a size of 6 nm in diameter. The sample with a size of 20×20 mm^2 was attached to the aluminum sample holder and installed in the Ps-TOF spectrometer. The positrons were implanted to the mesostructured sample. The XRD pattern of this mesoporous film is shown in Fig. 3.

The reference positron target was an open pored spin-on low-k film, consisting of zeolite nano-crystals. The porous

Table 1
Sample properties of the mesostructured sample as obtained with the XRD, TEM and the nitrogen gas absorption/desorption measurements

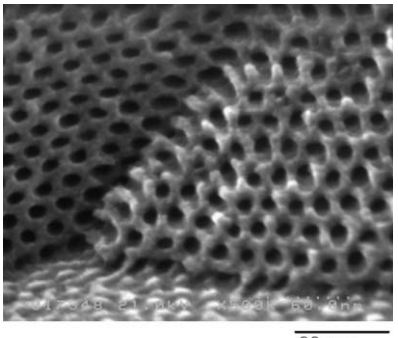

Sample thickness (nm)	200
Total porosity (%)	40
Pore size (nm)	6.0
Pore structure	2d cage-like
Lattice spacing (nm)	10.2
Density length (g/cm^3)	1.72×10^{-5}

FE-SEM image of the as-synthesized sample (scale bar, 60 nm; 500 k x) is shown.

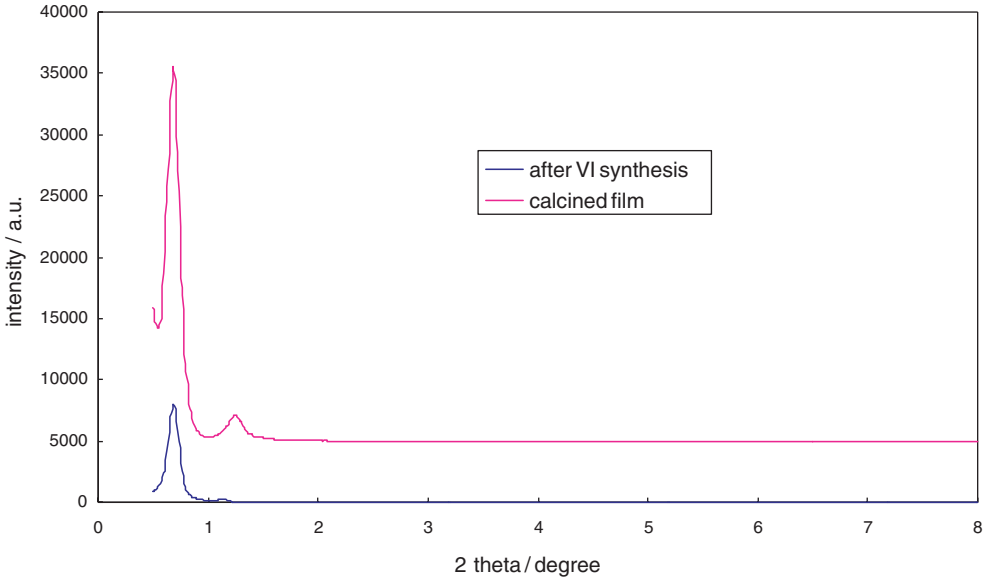

Fig. 3. XRD pattern of the as-synthesized sample (a). The XRD pattern of the calcined sample (b).

silica film sample was prepared under collaboration with Yan's laboratory, Bourns College of Engineering, University of California, Riverside. For the capped sample, the present films were prepared by a spin-on processes on Si wafers to form a porous film and a capping nonporous layer. The thickness of the porous layer was optimized for 3 keV positron (e^+) penetration through the capping and stopping in the porous layer [35]. The thickness and the porosity of each layer were measured by a spectroscopic wavelength ellipsometer (Jobin Yvon UVISEL Spectroscopic Phase Modulated Ellipsometer), and the pore diameter was measured by a nitrogen gas absorption/desorption method. The obtained values are shown in Table 2. The layer on top (Layer 1) is pure amorphous silica without any zeolite. The other two layers (Layers 2 and 3) are composed of both zeolite nano-crystals and amorphous silica. The thickness of the nonporous layer is ~50 nm. The porous layer with a thickness of ~220 nm has a gradual porosity distribution in Layer 2, ranging from 50.6% to 4.6% towards the nonporous layer, having the average porosity of 40.3%. The open-pored films were also prepared according to the same procedure. The thickness, the porosity of each layer and the pore size for the open-pored sample is summarized in Table 3.

Nitrogen adsorption/desorption measurements were conducted on powder samples by a Micromeritics ASAP 2010 analyzer. The observed pore size distribution was bimodal, which comprises the intrinsic zeolite microporosity of 5.5 Å in diameter and interparticle mesoporosity of

Table 2
Sample properties of the capped sample as obtained with the ellipsometer and nitrogen gas absorption/desorption measurements

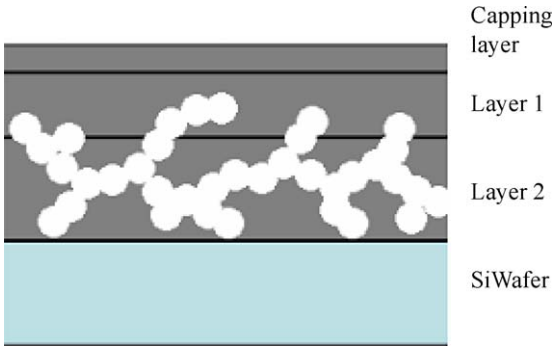

	Thickness (nm)	Porosity (%)	Pore size (nm)
Capping layer	52.3	4.6	4.0
Layer 1	83.0	40.3	4.0
Layer 2	144.8	50.6	4.0

Table 3
Sample properties of the open-pored sample as obtained with the ellipsometer and nitrogen gas absorption/desorption measurements

Sample thickness (nm)	431.7
Zeolite content (%)	38.3
Porosity in zeolite (%)	11.49
Porosity outside zeolite (%)	61.7
Total porosity (%)	73.19
Pore size (nm)	4, 0.5
Density length (g/cm^3)	2.55×10^{-5}

4 nm in diameter. The o-Ps lifetime of 50–60 ns, as obtained by assuming the rigid spherical potential model [34] is long enough to see the effect in a pore with a size of 4 nm in diameter. The sample with a size of 23 mm × 23 mm was attached to the aluminum sample holder and installed in the Ps-TOF spectrometer. The positrons were implanted to the porous layer through the nonporous layer.

3. Results and discussion

Figs. 4 and 5 show a positron implantation energy dependence of the Ps-TOF spectrum for various positron impact energies, ranging from 0.2 keV to 3.0 keV with a capped and open pored spin-on low-k film, and a new mesostructured film. In the present experiment, the difference between the positron transport energy (5 keV) and the voltage at the sample was employed as the positron energy at the sample. All the data were normalized to the measurement time (10,000 s). The prompt peak in Figs. 4 and 5 is a convolution of fast Ps decay events, which does not provide information about the nano-porous structure in the sample and neglected in the following discussion. The zero of time was fixed at the prompt peak. The width of the peak is due to the linac pulse width. The counts for $t < 0$ are associated with gamma rays and neutrons from the bremsstrahlung pair production target. The variations in Ps yield in these figures reflect each sample structure.

In Fig. 4, the Ps-TOF time spectra with positron implantation energies of 0.5 keV and 3.0 keV for an open-pored porous low-k film are shown. A large amount of long lifetime Ps component indicates the Ps escape into the vacuum. The major feature is a delayed component that is broadened and is delayed with positron implantation energy because Ps forms copiously in the porous layer, thermalizes and escapes through the interconnected porous network. The Ps diffusion time in the sample is negligible because $w^2/D \sim (300\ \text{nm})^2/(4\ \text{nm} \times 10^7\ \text{cm/s}) = 2 \times 10^{-10}$ s in the porous layer of a capped and open pored low-k sample is much less than the time of flight of ~100 ns. The Ps yield integrating over the time range 0–450 ns, which is independent on the positron implantation energy, is also consistent with $w^2/D \gg \tau_{4\ \text{nm}} \sim 50$ ns, where $\tau_{4\ \text{nm}}$ is the lifetime of the o-Ps.

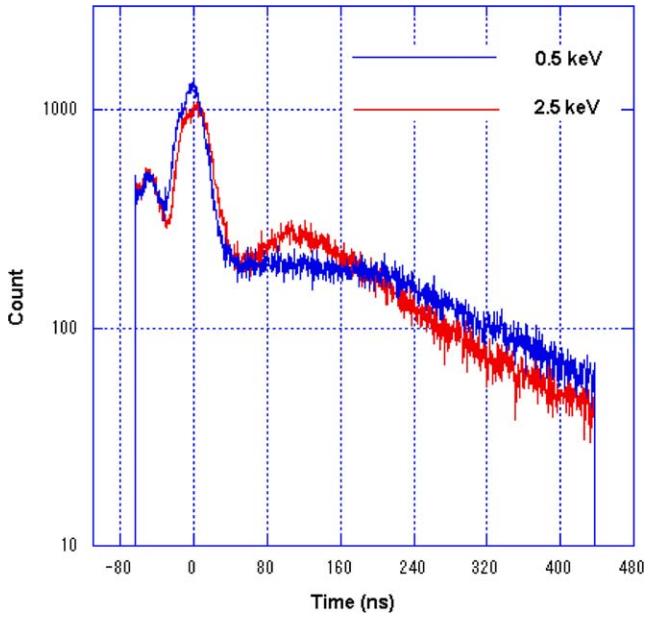

Fig. 4. Obtained Ps-TOF spectra in an open-pored low-k film with different incident positron energies of 0.5 keV and 2.5 keV. The distance between the sample and the detector slit is 45 mm. The zero of time was fixed at the prompt peak. The width of the peak is due to the linac pulse width. The counts for $t < 0$ are associated with gamma rays and neutrons from the bremstrahlung pair production target.

In Fig. 5, we compare the Ps-TOF spectra in the mesostructured film (Fig. 5(a)) to that in the capped film (Fig. 5(b)) with different positron implantation energies.

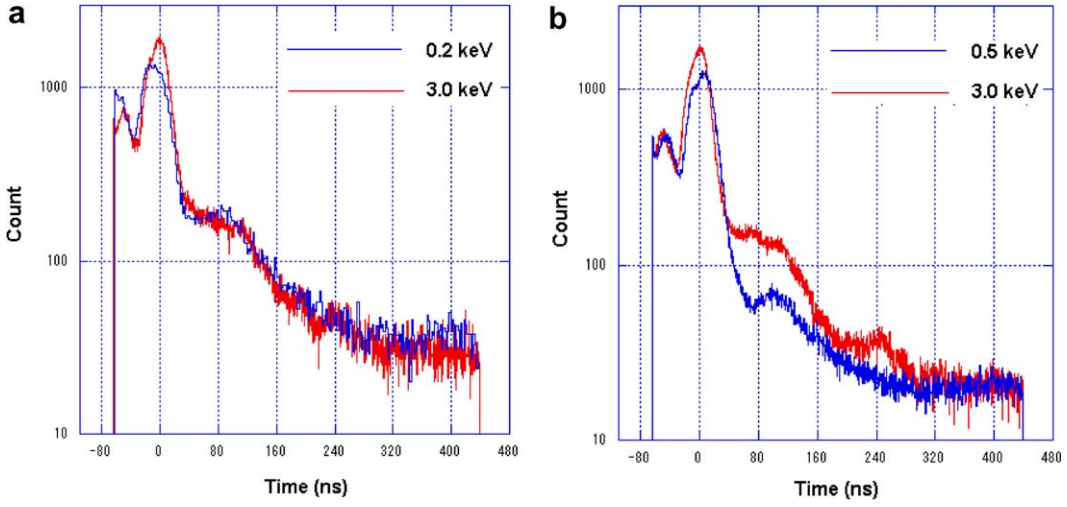

Fig. 5. Obtained Ps-TOF spectrum in (a) a mesostructured low-k film and (b) a capped low-k film with different incident positron energies, ranging from 0.2 keV to 3.0 keV. The distance between the sample and the detector slit is 45 mm. The zero of time was fixed at the prompt peak. The width of the peak is due to the linac pulse width. The counts for $t < 0$ are associated with gamma rays and neutrons from the bremstrahlung pair production target.

In the mesostractured sample, the shape and the Ps yield seem to be almost independent on the positron implantation energy indicating the periodical structure in the sample. The typical diffusion length of Ps in amorphous silica exceeds 10 nm, which is longer than the wall thickness of the present mesostructured sample. From our XRD analysis, as shown in Fig. 3, we think the porous structure is uniform. Thus, the Ps yield is independent of implantation energy, i.e. implantation depth as expected for a periodical structure. On the other hand, in the capped sample, the energy-dependent Ps-TOF spectra reflect the sample structure (Fig. 5(b)).

We now construct a picture of the positronium in our porous structure in order to interpret our data and arrive at an estimate for the fractional open area of its self-organized diffusion barrier by comparing it to the capped sample. Our picture of the various layers is as follows.

The multiple layers in the capped sample were used as a reference sample to examine the diffusion behavior of Ps confined beneath the artificial thicker amorphous diffusion barrier, i.e. the region in the layer 2 and the mixed porosity layer 1. In a capped sample, when the positrons are implanted into the middle of the capping layer using an implantation energy of 0.5 keV, they find themselves in an amorphous silica layer that forms positronium efficiently. Ps will diffuse to the surface and will be emitted into the vacuum with an energy of about 3 eV characteristic of the Ps negative affinity for amorphous silica as reported by Sferlazzo, Berko and Canter [36]. This Ps will be emitted essentially instantaneously compared to the relevant times of flight which are about 100 ns, thus leading to the small delayed peak at the positionium in Fig. 5(b).

In our new mesostructured film, even at very low energy, in this case 0.2 keV (<0.5 keV), the positron can penetrate through the first amorphous barrier Ps forms copiously in the porous, thermalizes and escapes through cracks or other gaps in the self-organized diffusion barrier. At high energies, in this case 3 keV, Ps forms copiously in both of the samples as shown in Fig. 5(a) and (b).

In a new mesostructured sample, positrons are implanted within the first few layers of the porous layer by giving them about 0.2 keV of implantation energy. The pore size is about $d = 6$ nm in diameter. The porous layer comprises a network of two-dimensionally interconnected cage-like pores that are parallel to the substrate. These pores are separated from each other with the self-organized thin diffusion barrier of $w = 5$ nm in thickness that is parallel to the substrate.

(a) We assume the self-organized diffusion barrier is almost impervious so that the Ps leakage rate out of the porous layer is small compared to its decay rate in the porous layer.
(b) The Ps mean thermal velocity v is such that d/v is much less than the time of flight of ~100 ns so that the Ps density is nearly constant throughout the porous layer: $t = d/v \approx (6\text{ nm})/10^7\text{ cm s}^{-1} = 10^{-13}\text{ s} \gg 100\text{ ns}$.
(c) It is thus clear that the rate of Ps leaking out of the porous region is the rate of an ideal gas hitting the diffusion barrier times the fractional open area η of the diffusion barrier. Thus the leak rate per positronium atom is $\Gamma = 1/4v\eta/d \approx 10^{13}\text{ s}^{-1} \times \eta$. It follows that the long time part of the time of flight curve (in the steady state limit) will have a characteristic lifetime that is the same as the lifetime of the Ps in the porous layer. This turns out to be about 60 ns, which is just the same as found in previous measurements on porous materials of similar characteristics, i.e. having 6 nm pores [34].
(d) Our assumption that the diffusion barrier is nearly impervious is consistent with the delayed 60 ns component seen in Fig. 5(a) for the 0.2 keV curve. It must therefore be that $\Gamma < (60\text{ ns})^{-1} = 1.7 \times 10^7\text{ s}^{-1}$. We therefore have an upper limit on the open area fraction:

$$\eta = \Gamma/10^{13}\text{ s}^{-1} < 1.7 \times 10^7\text{ s}^{-1}/10^{13}\text{ s}^{-1} = 1.7 \times 10^{-6}. \quad (1)$$

In conclusion, in the mesostructured film, at 0.2 keV, Ps forms copiously in the porous layer and thermalizes, but only very small number of Ps escapes through cracks or other gaps in an extremely thin self-organized diffusion barrier. In a capped sample, on the other hand, at 0.5 keV surface Ps escapes and gives us the small bump at about 100 ns time of flight as observed in Fig. 5(b). At 3 keV, in both of the samples, Ps forms copiously in the porous layer, thermalizes, and are confined beneath the diffusion barrier. In an open-pored porous low-k sample, a typical Ps-TOF time spectra as shown in Fig. 4 show a copious Ps formation thermalization and escape through an interconnected porous network.

Bose–Einstein condensation (BEC) effects of many positronium atoms (Ps; the electron bound state with its antiparticle, the positron) would be interesting to observe in a material in which there are a great many interconnected pores, such that Ps can diffuse over long distances (on the order of microns [8]). If we can confine the Ps in a very thin porous film by preventing escaping into vacuum, a dense Ps gas can be more easily produced. For the purpose of the production of a dense Ps gas, a diffusion barrier must be continuous and very thin, and the tradeoff between continuity and thickness of the barrier affects the Ps gas density in the porous layer underneath. It is therefore important to establish a method to characterize such film properties. At KEK-SPF, the positron beam is completely depolarized. If the positrons from which the positronium is formed are not perfectly spin polarized, there could be spin exchanging triplet positronium–triplet positronium collisions of dense Ps in the porous medium that would increase the average annihilation rate [37]. Our goal is an application of porous materials to fundamental physics to understand the structural effects of the sample that will enable us to optimize the barrier thickness as required for eventual measurements of spin exchange

cross section and possibly the Bose–Einstein condensation of Ps atoms.

In conclusion, a nano-architectural silica thin film with two-dimensionally connected cage-like pores has been characterized by using a Ps-TOF spectrometer. The measurements are consistent with the Ps produced in a porous layer being confined to the porous layer because of the low porosity of the self-organized diffusion barrier. The methodology for evaluating the diffusion barrier in the next generation low-k materials has been established.

Acknowledgments

The authors are grateful to Prof. Y. Yan and Dr. Z. Li for their powerful collaboration to prepare the capped low-k sample. The authors also acknowledge Prof. E.L. Chronister, and Dr. M. McIntire for valuable suggestions on porous materials. The authors are also grateful to Dr. H. Miyadera, Dr. D. Cassidy, Mr. R. Castillo-Garza, Mr. H. Imao, Mr. Y. Ikedo and Prof. K. Naganime for fruitful discussions about the present experiment. This work was supported in part by a Core to Core Program of JSPS. We are also grateful for financial support from the University of California Institute for Mexico and the United States (UC MEXUS).

References

[1] See, for example C. Jin, J.D. Luttmer, D.W. Smith, T.A. Ramos, MRS Bull. 39 (1997).
[2] The International Technology Roadmap for Semiconductors, International SEMATECH, Austin, TX, 2002.
[3] R.D. Miller, Science 286 (1999) 421–423.
[4] E. Kondoh, M.R. Baklanov, H. Bender, K. Maex, Electrochem. Solid State 1 (1998) 224–226.
[5] M. Morgen, E.T. Ryan, J.H. Zhao, C. Hu, T.H. Cho, P.S. Ho, Annu. Rev. Mater. Sci. 30 (2000) 645–680.
[6] B. Zhao, M. Brongo, Mater. Res. Soc. Symp. Proc. 565 (1999) 137.
[7] A.E. Kaloyeros, E. Eisenbraun, Ann. Rev. Mater. Sci. 30 (2000) 363.
[8] D.W. Gidley, W.E. Frieze, A.F. Yee, T.L. Dull, H.-M. Ho, E.T. Ryan, Phys. Rev. B, Rapid. Commun. 60 (1999) R5157.
[9] Shuang Li, Jianing Sun, Zijian Li, Huagen Peng, David Gidley, E. Todd Ryan, Yushan Yan, J. Phys. Chem. B 108 (2004) 11689–11692.
[10] J.N. Sun, D.W. Gidley, T.L. Dull, W.E. Frieze, A.F. Yee, E.T. Ryan, S. Li, J. Wetzel, J. Appl. Phys. 89 (2001) 5138.
[11] T.L. Dull, W.E. Frieze, D.W. Gidley, J.N. Sun, A.F. Yee, J. Phys. Chem. B 105 (2001) 4657.
[12] Jia-Ning Sun, Yifan Hu, William E. Frieze, Wei Chen, David W. Gidleya, J. Electrochem. Soc. 150 (5) (2003) F97–F101.
[13] R. Tuomisaari, H. Howell, T. McMullen, Phys. Rev. B 40 (1989) 2060.
[14] A.P. Mills Jr., L. Pfeiffer, Phys. Rev. Lett. 43 (1979) 1961–1964.
[15] M. Ogawa, J. Am. Chem. Soc. 116 (1994) 7941–7942.
[16] I.A. Aksay, M. Trau, S. Manne, I. Honma, N. Yao, L. Zhou, P. Fenter, P.M. Eisenberger, S.M. Gruner, Science 273 (1996) 892–898.
[17] H. Yang, N. Coombs, I. Sokolov, G.A. Ozin, Nature 381 (1996) 589–592.
[18] H. Yang, A. Kuperman, N. Coombs, S. Mamich-Afara, G.A. Ozin, Nature 379 (1996) 703–705.
[19] H. Yang, N. Coombs, I. Sokolov, G.A. Ozin, J. Mater. Chem. 7 (1997) 1285–1290.
[20] N. Nishiyama, A. Koide, Y. Egashira, K. Ueyama, Chem. Commun. (1998) 2147–2148.
[21] Y. Lu, R. Ganguli, C.A. Drewien, M.T. Anderson, C.J. Brinker, W. Gong, Y. Guo, H. Soyez, B. Dunn, M.H. Huang, J.I. Zink, Nature 389 (1997) 364–368.
[22] A. Sellinger, P.R. Weiss, A. Nguyen, Y. Lu, R.A. Assink, W. Gong, C.J. Brinker, Nature 394 (1998) 256–260.
[23] J.C. Vartuli, K.D. Schmitt, C.T. Kresge, W.J. Roth, M.E. Leonowicz, S.B. McCullen, S.D. Hellring, J.S. Beck, J.L. Schlenker, D.H. Olson, E.W. Sheppard, Chem. Mater. 6 (1994) 2317–2326.
[24] Q. Huo, R. Leon, P.M. Petroff, G.D. Stucky, Science 268 (1995) 1324–1327.
[25] S. Inagaki, Y. Fukushima, K. Kuroda, J. Chem. Soc. Chem. Commun. (1993) 680–682.
[26] D. Zhao, J. Feng, Q. Huo, N. Melosh, G.H. Fredrickson, B.F. Chmelka, G.D. Stucky, Science 279 (1998) 548–552.
[27] D. Grosso, F. Babonneau, G.J.A.A. Soler-Illia, P. Albouy, H. Amenitsch, Chem. Commun. (2002) 748–749.
[28] M.C. Liu, H.S. Sheu, S. Cheng, Chem. Commun. (2002) 2854–2855.
[29] Q. Huo, D.I. Margolese, G.D. Stucky, Chem. Mater. 8 (1996) 1147–1160.
[30] N. Nishiyama, S. Tanaka, Y. Egashira, Y. Oku, K. Ueyama, Chem. Mater. 15 (2003) 1006–1011.
[31] Shunsuke Tanaka, Norikazu Nishiyama, Yoshiaki Oku, Yasuyuki Egashira, Korekazu Ueyama, J. Am. Chem. Soc. 126 (2004) 4854–4858.
[32] T. Kurihara, A. Shirakawa, A. Enomoto, T. Shidara, H. Kobayashi, K. Nakahara, Appl. Surf. Sci. 85 (1995) 178.
[33] Y. Morinaka, Y. Nagashima, Y. Nagai, T. Hyodo, T. Kurihara, T. Shidara, K. Nakahara, in: Y.C. Jean, Morten Eldrup, David M. Schrader, Roy N. West (Eds.), Positron Annihilation – ICPA-11, Trans Tech Publications, Switzerland, 1997, pp. 689–691.
[34] Kenji Ito, Hiroshi Nakanishi, Yusuke Ujihira, J. Phys. Chem. B. 103 (1999) 4555–4558.
[35] A.P. Mills Jr., Robert J. Wilson, Phys. Rev. A 26 (1982) 490.
[36] P. Sferlazzo, S. Berko, K.F. Canter, Phys. Rev. B 35 (1987) 5315.
[37] See pp. 253–254 of A.P. Mills Jr., Positron and positronium emission spectroscopies, in: A. Dupasquier, A.P. Mills Jr. (Eds.), Positron Spectroscopy of Solids, IOS Press, 1995, pp. 209–258.